Materials Science & Engineering A 756 (2019) 313–318

Contents lists available at ScienceDirect

Materials Science & Engineering A

journal homepage: www.elsevier.com/locate/msea

Spatiotemporal correlations in the Portevin-Le Chatelier band dynamics during the type B - type C transition

M. Mehenni[a], H. Ait-Amokhtar[a,*], C. Fressengeas[b]

[a] Laboratoire de Physico-Chimie des Matériaux et Catalyse (LPCMC), Faculté des Sciences Exactes, Université de Bejaia, 06000 Bejaia, Algeria
[b] Laboratoire d'Etude des Microstructures et de Mécanique des Matériaux (LEM3), Université de Lorraine/CNRS/Arts et Métiers ParisTech, 7 rue Félix Savart, Metz 57070, France

ARTICLE INFO

Keywords:
Aluminum alloys
Portevin-Le Chatelier effect
Dynamic strain aging
Plastic instability
Infrared thermography

ABSTRACT

The spatiotemporal aspects of the Portevin-Le Chatelier (PLC) instability are investigated, using infrared thermography, in an Al-4.5%Mg alloy loaded at room temperature in simple tension at an imposed strain rate such that a transition from type B to type C bands occurs during the test. By following the evolution in time of the band characteristics, the analysis reveals a close correlation between the dynamics of band nucleation and the organization of stress serrations during the type B-type C transition as strain increases. The initially small and regular stress drops become less regular, more dispersed and exhibit a larger magnitude across this transition. In the type B regime, new bands nucleate at constant frequency ahead of the previous one, with a band spacing slightly smaller than the bandwidth, giving an impression of continuous band propagation, although the bands are actually static. After the transition, the band spacing becomes much larger than the bandwidth, suggesting a trend to random nucleation in space. Similarly, the statistical distribution of the stress drops size evolves towards a more symmetrical peak-shaped Gauss-type distribution across the transition. These results are discussed in accordance with dynamic strain aging interpretations.

1. Introduction

Jerky flow is an unstable and heterogeneous plastic flow commonly observed in metallic materials, particularly in Al-Mg alloys [1–5]. At microscopic scale, it originates in the Portevin-Le Chatelier (PLC) effect, i.e. a Dynamic Strain Aging (DSA) phenomenon involving a dynamic interaction between solute atoms and mobile dislocations [6–8]. When the characteristic diffusion time of the solute atoms is of the order of the waiting time t_w of dislocations temporarily arrested at localized obstacles (precipitates, forest dislocations, etc.), these atoms are able to diffuse to and age arrested dislocations. Consequently, the strength of the obstacles to dislocation motion increases, as well as the flow stress. Such pinning of dislocations by the solute atoms increases with t_w, i.e. when the applied strain rate decreases, and/or when the characteristic time of solute diffusion decreases by temperature increase. Hence, DSA reduces the Strain Rate Sensitivity (SRS) of the flow stress, which may become negative in some range of strain, strain rate and temperature. Under such conditions, the homogeneous plastic flow becomes unstable and strain localizes into narrow deformation bands correlated with serrations in the stress-strain curves at constant applied strain rate [1–6,9–12]. The PLC effect has been studied experimentally using various methods, such as direct observations by video recordings [1,9], optical methods [9,12,13], digital image correlation [5,14] and infrared thermography [2–5,11]. In Al-Mg alloys, which provide a large variety of applications due to their low weight and high mechanical strength, the PLC effect occurs around room temperature and in limited ranges of strain and strain rate [5,6,9,10]. Its characteristics (domain of the instability, magnitude of the stress drops, etc.) depend on the thermo-mechanical manufacturing history of the deforming material [10,12,15]. Depending on deformation conditions, three types of PLC instabilities (see Fig. 1), producing three distinct kinds of strain localization patterns, can be observed at constant applied strain rate [1–3,5,9]. Type A instabilities appear at large strain rates in the form of weak undulations on the stress-strain curves, and are associated with strain localization characterized by continuous band propagation, due to strong spatial correlations. The associated serrations display a large variety of magnitudes. Type B instabilities occur at intermediate strain rates. They manifest themselves as drops of the stress below the level of the stable flow stress. The spatial correlations are reduced with respect to type A, as will be explained below. They lead to static but apparently propagating associated bands ("hopping bands") and to more typical serrations on the stress-strain curves. Type C instabilities occur at very

* Corresponding author.
E-mail addresses: hakim.ait-amokhtar@univ-bejaia.dz, hakim.aitamokhtar@gmail.com (H. Ait-Amokhtar).

https://doi.org/10.1016/j.msea.2019.04.036
Received 19 February 2019; Received in revised form 3 April 2019; Accepted 8 April 2019
Available online 09 April 2019
0921-5093/

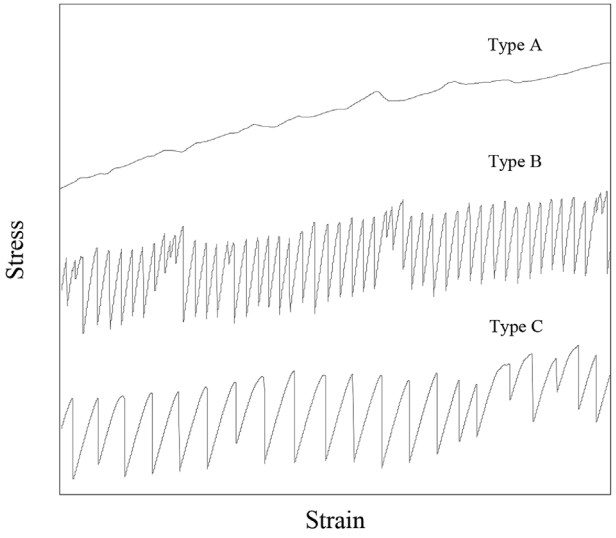

Fig. 1. Typical fragments of stress-strain curves demonstrating the three commonly observed types of PLC instabilities with a hard testing machine, i.e. at constant driving velocity. The instability changes from type A to type B then to type C when decreasing the imposed strain rate and/or increasing the temperature.

low strain rates and produce larger serrations on the stress-strain curves as compared with types A and B, with drops and overloads around the average flow stress value. The associated bands are static and nucleate randomly on the deformed material due to still weaker spatial correlations. Jerky flow theoretical analyses [16–18] suggest that the spatial correlation between plasticity events is due to internal stresses arising from lattice distortion incompatibility in the bands areas. Changes in material deformation conditions lead to variations in the degree of spatial correlation between plastic events and, consequently, to shifts in the PLC dynamical regime. As indicated above, the band type changes from type A to type B then to type C when decreasing the imposed strain rate and/or increasing temperature [1,9,13]. These transitions may also be observed in a single test at constant strain rate and temperature when strain increases [4,5,9–11,19]. The band type may then shift from type A to type B [4,5,19] and from type B to type C [9,11] with increasing strain. This last transition has not been extensively studied in the literature and will be the focus of the present investigation. In particular, we will quantitatively characterize the transition using our measurements of the band characteristics, and interpret the results in terms of DSA mechanisms [6–8]. Studying the PLC bands dynamics during the type B - type C transition should lead to a better understanding of these mechanisms and, consequently, should allow optimizing the parameters of homogeneous processing and forming of Al-Mg alloys.

In this aim, we used infrared thermography, and analyzed the spatiotemporal aspects of PLC bands in a test at the constant applied strain rate $2.38 \times 10^{-4}\ s^{-1}$ and at room temperature in an Al-4.5%Mg alloy. In such conditions, the instability changes from type B to type C with increasing strain. Through the analysis of the temperature fields, we study the band dynamics and characteristics in connection with the organization of the associated stress drops on the stress-time curve.

2. Experimental

The material used in the present study is an Al-4.5%Mg alloy. Its nominal chemical composition in weight percent is given in Table 1. Polycrystalline flat specimens (gauge length 70 mm, width 10 mm, thickness 1 mm) were machined in the rolling direction and deformed in tension at room temperature (25 °C) with a hard testing machine, i.e. at constant driving velocity and strain rates in the range 10^{-6}-10^{-1} s^{-1}, corresponding to the domain of PLC instability in the present alloy [9].

Table 1
Chemical composition of the Al-4.5%Mg alloy (in wt.%).

Alloy	Mg	Mn	Si	Fe	Cu	Zn	Ti	Cr
Al-4.5%Mg	4.45	0.42	0.40	0.41	0.10	0.25	0.15	0.05

In addition to the mechanical device, which allows recording the applied load and the overall displacement, an infrared camera (CEDIP JADE III MW) was used to simultaneously record the temperature field of the sample surface during straining. The temperature fields were obtained at a frequency of 145 Hz and with a spatial resolution of 320 × 240 pixels. The very low noise level of the camera, less than 0.02 °C, allowed detecting even the small variations of temperature associated with weak fluctuations of the plastic deformation [3,20]. In order to minimize the errors associated with pyrometry and calibration, the surface of the samples was covered with a strongly emissive black painting.

In the following, we present and analyze thoroughly the results obtained at the strain rate $2.38 \times 10^{-4}s^{-1}$ and we will refer to the other tests, performed in the range 10^{-6}-10^{-1} s^{-1}, to analyze the effects of strain rate changes on jerky flow. At $2.38 \times 10^{-4}\ s^{-1}$, with the focal distance of the lenses we used, the pixel size was 0.35 mm. This elementary distance was used to quantify the distribution in space of the measured temperature values, from which geometric band characteristics such as the bandwidth or the band spacing will be derived. As the temperature variations due to PLC band nucleation remain weak, less than 1.2 °C, the temperature fields will be given as differences with the equilibrium room temperature of the sample before straining.

3. Results and discussion

3.1. PLC band dynamics during the type B-type C transition

In the deformation conditions we imposed, at room temperature and for applied strain rates ranging from 10^{-6} to 10^{-1} s^{-1}, the Al-4.5%Mg alloy is subject to unstable plastic flow. The macroscopic SRS of the flow stress was found to be negative and a decreasing function of strain. In tests carried out in the strain rates sub-domain 10^{-6}-$6 \times 10^{-4}\ s^{-1}$, stress drops are large (10–30 MPa) and accompanied by intense audible acoustic emission. The associated plastic strain localization leaves traces on the sample surface that are visible with a naked eye. Fig. 2 shows the serrated stress-time curve at room temperature and the strain rate of $2.38 \times 10^{-4}\ s^{-1}$. The figure clearly highlights the effects of strain on the stress drops whose magnitude is indicative of the degree of heterogeneity of plastic flow and is closely related with the effectiveness of DSA. In the early stages of serrated flow, the instabilities are of type B, the stress drops are regular and of a relatively small size. After the transition to type C, obtained by increasing strain, the stress drops have a larger but less typical size, implying that DSA has become more efficient. Fig. 2 shows indeed that the stress drops magnitude exhibits more dispersion as the strain increases, suggesting a reduction in the degree of spatial correlation between plasticity events in the material [16–18].

During the test, four temperature field recordings were carried out from times $t_1 = 295.08$ s, $t_2 = 320.58$ s, $t_3 = 344.04$ s and $t_4 = 459.28$ s onwards during almost 6.90 s. Each insert in Fig. 2 represents a domain where a temperature field record of 1000 images was carried out. The stress drops corresponding to the recorded localized deformation bands are highlighted in the figure by using a bold line. From the identical dimensions of the four inserts, it is seen that the magnitude of the stress drops and the reloading time between two successive stress drops increase with time.

In order to analyze the kinetics of a PLC band nucleation, we

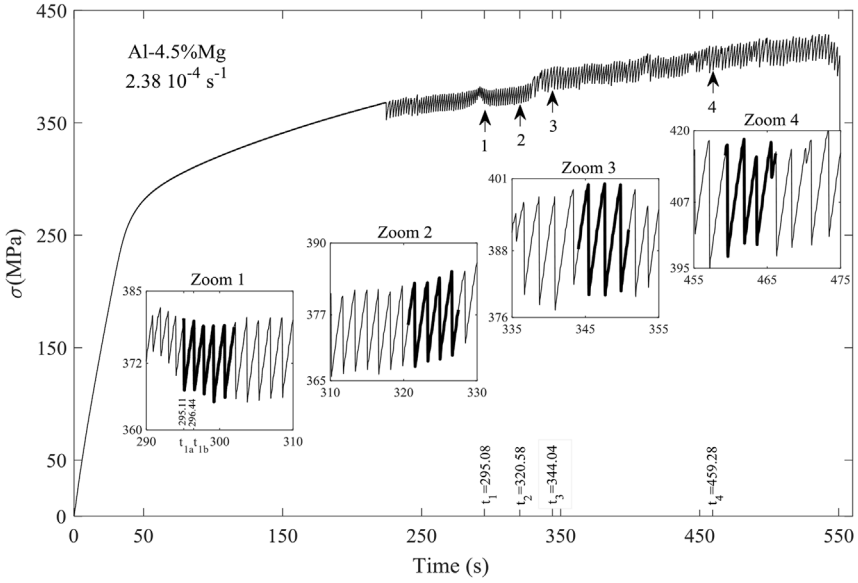

Fig. 2. Stress-time curve showing PLC instabilities at room temperature in an Al-4.5%Mg alloy deformed at a strain rate of 2.38×10^{-4} s^{-1}. Inserts: Close-ups showing the domains, of the same dimension (20 s × 25 MPa), where the temperature fields are recorded from times t_1, t_2, t_3 and t_4 onwards. Stress drops corresponding to the recorded localized deformation bands are highlighted by using a bold line.

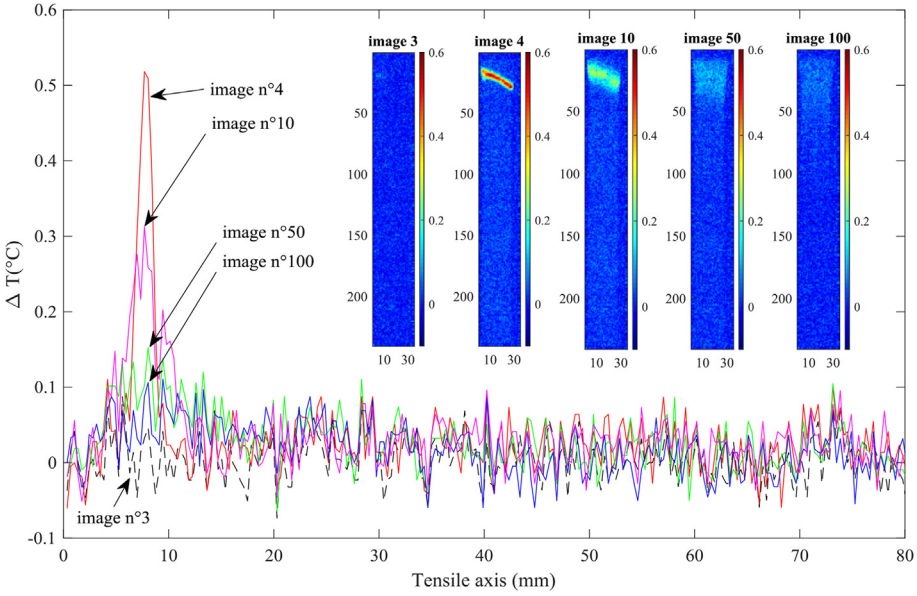

Fig. 3. Evolution in time (five images) of the temperature increment field along the tensile axis showing the abrupt occurrence of a type B PLC band (image 4) in an Al-4.5%Mg alloy at the strain rate of 2.38×10^{-4} s^{-1}. Insert: Full images of the temperature increment field on the sample surface. Note the effects of heat diffusion and the transfer off the sample of the heat produced by strain localization.

consider the first band recorded at time t_{1a} = 295.11s in the first temperature field record (see insert 1 in Fig. 2). The temperature increments fields of the sample surface and the temperature variations produced along the tensile axis during the formation of the band are reported in Fig. 3. The figure shows the sharp appearance of a localized increase in temperature in the form of a narrow strip (image 4 in the insert) and, later on, the diffusion and transfer off the sample of the heat produced by strain localization. The band nucleates abruptly at an angle of 62 ± 0.1° to the tensile axis in less than 6.9 ms (1/145s), between images 3 and 4. After band formation at time t_{1a} = 295.11 s, the local temperature decreases progressively down to the equilibrium value in less than 0.7s (around image 100). The next band appears elsewhere at time t_{1b} = 296.44s, i.e. 1.33s after the first band nucleation and 0.6s after homogenization and return of the temperature field to its equilibrium value. Fig. 3 highlights the static character of the type B bands: band nucleation produces a locally pronounced increase in the temperature field, whose decay occurs without propagation along the sample. This temperature evolution also suggests that strain localization in the area of sharp temperature increase is accompanied by elastic unloading in the rest of the sample. Note in contrast that in the case of type A bands, the temperature peak stops increasing after band nucleation, and thereafter the band propagates by widening [2].

Fig. 4 shows the abrupt and localized increases in the temperature fields corresponding to consecutive band nucleation events along the tensile axis from times t_1, t_2, t_3 and t_4 onwards. The instants of band occurrence are also reported in each record. In the first and second records (Fig. 4a and b), which were performed in the early stages of serrated flow, we observed respectively five and four consecutive localized deformation bands. Each band is static, but nucleates ahead of the previous one leading to apparent propagation of the localization area and to regular stress drops with a relatively small size (see Fig. 2). The frequency of band occurrence is almost constant and, therefore, the localization areas move in the same direction with constant velocities 0.99 ± 0.01 mm/s and 0.68 ± 0.01 mm/s, respectively. This behavior is characteristic of type B bands [1–5], which are consequently referred to as “hopping bands”. Using the digital image correlation method [14], we had found in the same alloy and strain domain an apparent “band velocity” of 0.12 mm/s and 0.53 mm/s, respectively at the strain rate of 4.05×10^{-5} s^{-1} and 1.6×10^{-4} s^{-1}. These results show that the apparent type B band velocity increases with the imposed strain rate and

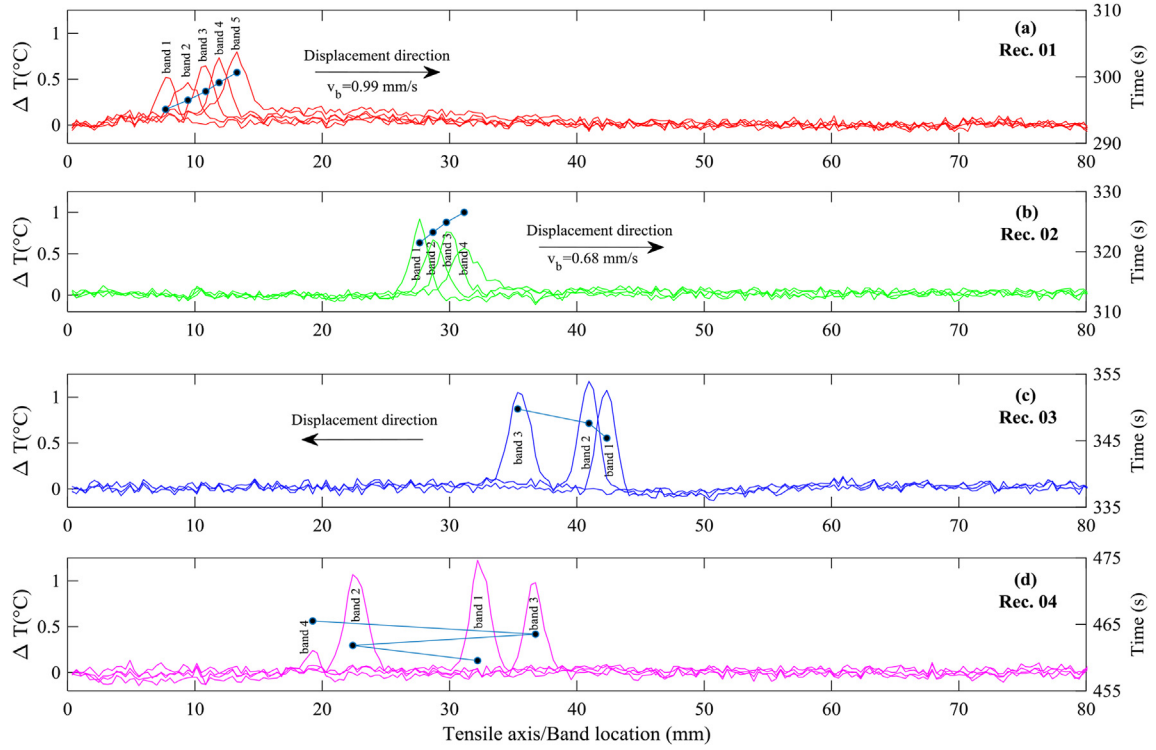

Fig. 4. Temperature profiles along the tensile axis in the Al-4.5%Mg alloy at the strain rate of $2.38 \times 10^{-4}\ s^{-1}$, showing the nucleation of consecutive PLC bands on the sample surface, starting respectively from times $t_1 = 295.08$ s (a), $t_2 = 320.58$ s (b), $t_3 = 344.04$ s (c) and $t_4 = 459.28$s (d). Superimposed is the corresponding time of band appearance indicated by the symbol • (see right y-axis).

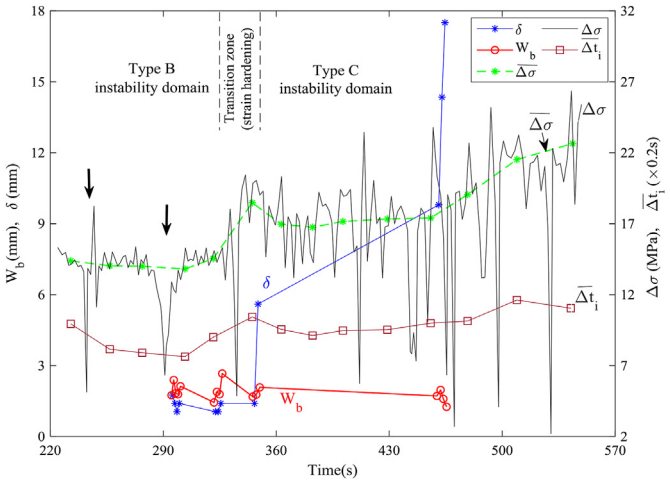

Fig. 5. Time dependence of the bandwidth W_b and band spacing δ between two consecutive bands in an Al-4.5%Mg alloy at the strain rate of $2.38 \times 10^{-4}\ s^{-1}$ (see left y-axis). Superimposed are the magnitude of the stress drops Δσ vs. time, and its average value $\overline{\Delta\sigma}$, and the average reloading time between two successive stress drops $\overline{\Delta t_i}$, during the entire test when instabilities shift from type B to type C (see right y-axis).

decreases with strain at constant applied strain rate.

In the third record (see Fig. 4c), the band locations in space and time clearly indicate that the apparent velocity of the hopping band is no more constant. Both band jumps are in the same direction with velocities of −0.63 mm/s and −2.59 mm/s, respectively. In the fourth record (see Fig. 4d), the bands appear randomly with variable frequency and, therefore, exhibit non-constant jump velocities −4.29, +8.46 and −8.81 mm/s in either directions, respectively. This behavior is characteristic of type C bands [1,4,9,18]. Note that the smallest band in Fig. 4d (band 4) is correlated with a small stress drop in the stress-time curve (insert 4 in Fig. 2).

As suggested earlier, the temperature bursts originate in the dissipation of mechanical work due to localized jumps in the plastic strain rate. During band formation, the strain rate within the active band jumps from the applied strain rate $\dot{\varepsilon}_a$ to the localized value $\dot{\varepsilon}_{Loc} = \alpha\, \dot{\varepsilon}_a$. The parameter α measures the intensity of localization. Assuming adiabaticity during band formation, i.e. neglecting heat conduction and transfer, the temperature bursts allow estimating α (see Ref. [2] for the calculation details). From the heat equation, written inside the active band, we find the average α values 5607, 6429, 9345 and 8869 (the small band in the fourth recording being excluded) for the four generations of bands shown in Fig. 4 respectively. These results are consistent with our earlier reports in the Al-3.2%Mg alloy, at the same applied strain rate of $2.38 \times 10^{-4}\ s^{-1}$ using infrared thermography [2], and in the Al-4.5%Mg alloy, at the applied strain rate of $1.6 \times 10^{-4}\ s^{-1}$, using a white light interferometer [9]. The increasing average value of the localization intensity factor α indicates that the localization of plastic flow becomes more intense and suggests again that DSA becomes more effective when strain increases.

3.2. PLC band characteristics and stress drop distributions

The geometrical characteristics of the PLC bands are now estimated from the temperature fields corresponding to their formation. The band angle with respect to the tensile axis ranges from 58° to 62°, which is in accordance with previous experimental reports [1,2,5,11,12]. As the temperature is not uniform inside the band (see Fig. 3), we define the bandwidth at the half height of the localized peak in temperature at band nucleation [2,11]. Since the temperature peak widens after the abrupt appearance of the band, due to heat diffusion and transfer off the sample, the error in bandwidth measurement can be estimated to 0.15 mm. This value corresponds to the maximal variation in the peak width between two successive images after band formation. For the four generations of bands reported in Fig. 4, at the strain rate of

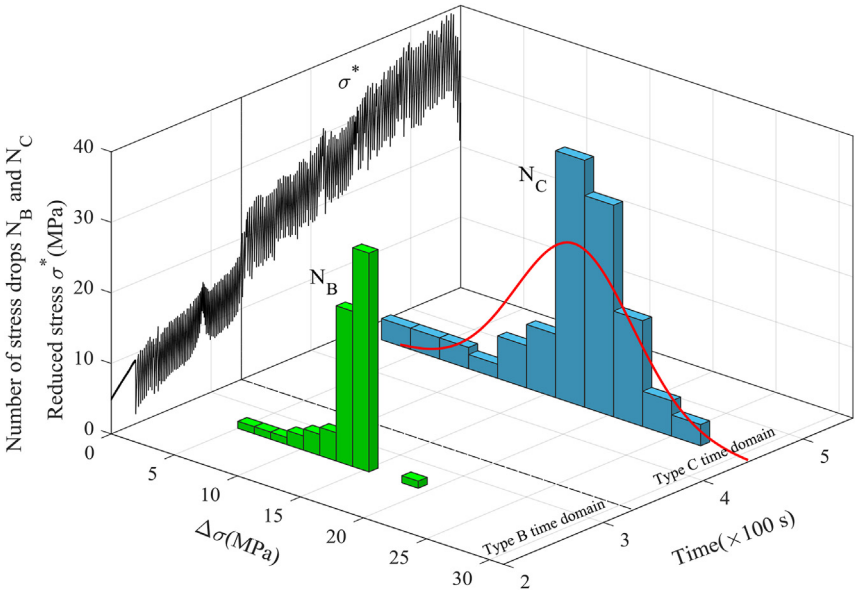

Fig. 6. Evolution in time of the statistical distributions of stress drops in an Al-4.5%Mg alloy at the applied strain rate of $2.38 \times 10^{-4}\ s^{-1}$. N_B: statistical distribution at low strains domain (type B); N_C: statistical distribution at large strains domain (type C). To show in parallel the instability pattern, the reduced stress $\sigma^* = (\sigma\text{-}350)/2$ curve is plotted vs. time using the same axis.

$2.38 \times 10^{-4}\ s^{-1}$, we find respectively an average bandwidth of 1.97, 1.94, 1.84 and 1.63 mm, showing a decreasing trend when strain increases, which suggests again more intense strain localization. This result is in agreement with earlier reports on Al-Mg alloys using optical measurements [9,12].

Fig. 5 shows the time dependence of the bandwidth W_b and band spacing δ between the centers of two consecutive bands, for the bands recorded in the four temperature fields shown in Fig. 4. Evolutions of the magnitude of the stress drops Δσ, its average value $\overline{\Delta\sigma}$ and the average reloading time between two successive stress drops $\overline{\Delta t_i}$, during the entire tensile test, are also reported in this figure. In the type B time domain, W_b is slightly larger than δ indicating some overlap of the bands. As already indicated, each new static band nucleates ahead of the previous one, but partly overlaps the latter, giving the impression of a single progressing band. At the transition from type B to type C, the gap δ between bands becomes much larger than the bandwidth W_b, which suggests that type C bands occur in a spatially uncorrelated manner. Indeed, band nucleation faraway from the previous band suggests randomness in space of the nucleation process. In addition, Fig. 5 shows that in the type B domain, the magnitude of the stress drops Δσ fluctuates only slightly for the same generation of bands (1–2 MPa). The two large drops indicated by arrows are associated with the end of a generation of bands and the starting point of the next one, usually at a different location and after a small amount of hardening (see Fig. 2). In the type C domain, the stress serrations are less regular. They display both drops and overloads above the average value $\overline{\Delta\sigma}$ indicated by a green dashed line. Further, the serrations display a larger magnitude and exhibit more dispersion with respect to $\overline{\Delta\sigma}$. This trend suggests again that DSA enhances with increasing strain. The reasons for this increased efficiency of solute pinning can be found in the increase with strain of the dislocation densities, and possibly with an improved diffusivity of the solute atoms.

Fig. 5 shows that in the type B and type C domains, the average reloading time between two successive stress drops $\overline{\Delta t_i}$ varies slightly with time. When the instabilities change from type B to type C, $\overline{\Delta t_i}$ performs a jump from a lower plateau to an upper one. This result is consistent with the observed change in the dynamics of band nucleation and the organization of stress serrations during the type B-type C transition (see Fig. 4), and it confirms our earlier reports in the Al-2.5% Mg alloy, at the applied strain rate of $1.9 \times 10^{-5}\ s^{-1}$, and in the Al-4.5%Mg alloy, at the applied strain rate of $4 \times 10^{-5} s^{-1}$ [9].

Earlier analyses of the stress drops statistics at various applied strain rates [16,21,22] showed correlations between the type of instability and the character of the associated statistical distributions of the stress drops magnitude. Fig. 6 shows the evolution in time of the statistical distributions of stress drops when the instability shifts from type B to type C during straining. In the initial stage of serrated flow (type B), the stress drop distribution N_B displays a prevalence of very typical drops in the range 25–30 MPa. Both smaller and larger drops can be observed, but in very small numbers. Beyond the transition, which can be visually identified in the figure from the shift in the morphology of the serrations in the stress vs. time curve, from drops below the stable flow stress level to drops and overloads around the average flow stress value, the stress drop distribution N_C exhibits more dispersion with a trend to more symmetrical bell-shaped distribution. This evolution suggests again uncorrelated occurrence of type C bands and weaker spatial correlations at large strains [16,21,22], whereas the distribution N_B is more undecided, due to the small numbers of untypical events, but is compatible with stronger spatial correlations in type B.

To sum up our results, the type B-type C transition (as commonly determined visually from the shift in the morphology of the stress serrations) can be accurately quantified from the bandwidth, band spacing and stress vs. time measurements shown in Figs.(2), (5) and (6). Whereas the band spacing is slightly smaller than the bandwidth in type B, indicating rather closely correlated and partly overlapping bands, it becomes much larger than the bandwidth at the transition to type C, thereby suggesting uncorrelated band occurrence. The statistical distributions plotted in Fig. 6, where a similar trend to symmetrical Gauss-type bell-shaped distributions can be found at large strains, confirm this trend to uncorrelated plastic events as strain increases. In addition, the temperature field measurements shown in Fig. 4 allow documenting the shifts in the dynamical regime across this transition. Fig. 4 also allows fully describing the hopping band propagation mechanism pertaining to the type B dynamical regime: all bands are static bands, but as each new band nucleates ahead of (and partly overlaps) the previous one, the whole process gives the impression of a single propagating band.

4. Concluding remarks

Using temperature field measurements performed by infrared thermography, we studied some spatiotemporal aspects of the Portevin-Le Chatelier effect in an Al-4.5%Mg alloy at room temperature. Band characteristics were measured in a single test carried out at the applied strain rate $2.38 \times 10^{-4}\ s^{-1}$, in the course of which the instabilities shift from type B to type C with increasing strain. The results clearly show a close relationship between the organization of the stress drops on the

stress-time curve and the dynamics of the bands during the type B to type C transition. They also allow to accurately pinpoint in strain the type B-type C transition. The bands are static throughout the test, but in the early stage of serrated flow, i.e. in the type B domain, the bandwidth is slightly larger than the band spacing, which is consistent with bands hopping ahead of one another. After the transition to type C, the band spacing becomes much larger than the bandwidth, which reflects bands occurring in a spatially uncorrelated manner. In addition, the stress serration size exhibits more dispersion and its statistical distribution evolves towards a Gauss-type bell-shaped distribution, also suggesting uncorrelated occurrence of the bands. These results are consistent with the interpretation set forth earlier in Ref. [9]: as strain increases during the test, the obstacles to dislocation motion (such as forest dislocations) become more and more difficult to overcome. Consequently, the reloading time between consecutive stress serrations and the serration amplitude increase. Thus, both the frequency of the occurrence of bands and their apparent velocity decrease, as shown above from Fig. 4. As there is more time available during reloading for plastic relaxation of the internal stresses, spatial coupling deriving from the latter becomes weaker, which explains the shift from apparent band propagation in type B to static uncorrelated bands in type C dynamics.

Acknowledgments

The experiments reported in this paper were performed at the University of Savoie (France). The temperature field measurements were conducted with the help of H. Louche, who is gratefully thanked. H. Ait-Amokhtar would also like to thank LEM3 for welcoming and helping him during several visits.

References

[1] K. Chihab, Y. Estrin, L.P. Kubin, J. Vergnol, The kinetics of the Portevin-Le Chatelier bands in an A1-5at%Mg alloy, Scripta Metall. 21 (1987) 203–208.
[2] H. Ait-Amokhtar, C. Fressengeas, S. Boudrahem, The dynamics of Portevin-Le Chatelier bands in an Al-Mg alloy from infrared thermography, Mater. Sci. Eng. A. 488 (2008) 540–546.
[3] H. Louche, P. Vacher, R. Arrieux, Thermal observations associated with the Portevin-Le Châtelier effect in an Al-Mg alloy, Mater. Sci. Eng. A. 404 (2005) 188–196.
[4] N. Ranc, D. Wagner, Experimental study by pyrometry of Portevin-Le Châtelier plastic instabilities-Type A to type B transition, Mater. Sci. Eng. A. 474 (2008) 188–196.
[5] H. Ait-Amokhtar, C. Fressengeas, Crossover from continuous to discontinuous propagation in the Portevin-Le Chatelier effect, Acta Mater. 58 (2010) 1342–1349.
[6] L.P. Kubin, Y. Estrin, Dynamic strain ageing and the mechanical response of alloys, J. Phys. III 1 (1991) 929–943.
[7] A. Van den Beukel, Theory of the effect of dynamic strain aging on mechanical properties, Phys. Stat. Sol. (a) 30 (1975) 197–206.
[8] P.G. McCormick, A model for the Portevin-Le Chatelier effect in substitutional alloys, Acta Metall. 20 (1972) 351–354.
[9] H. Ait-Amokhtar, S. Boudrahem, C. Fressengeas, Spatiotemporal aspects of jerky flow in Al-Mg alloys, in relation with the Mg content, Scripta Mater. 54 (2006) 2113–2118.
[10] L. Ziani, S. Boudrahem, H. Ait-Amokhtar, M. Mehenni, B. Kedjar, Unstable plastic flow in the Al-2%Mg alloy, effect of annealing process, Mater. Sci. Eng. A 536 (2012) 239–243.
[11] N. Ranc, D. Wagner, Some aspects of Portevin-Le Chatelier plastic instabilities investigated by infrared pyrometry, Mater. Sci. Eng. A. 394 (2005) 87–95.
[12] R. Shabadi, S. Kumar, H.J. Roven, E.S. Dwarakadasa, Characterisation of PLC band parameters using laser speckle technique, Mater. Sci. Eng. A 364 (2004) 140–150.
[13] L. Casarotto, R. Tutsch, R. Ritter, J. Weidenmüller, A. Ziegenbein, F. Klose, H. Neuhäuser, Propagation of deformation bands investigated by laser scanning extensometry, Comp. Mater. Sci. 26 (2003) 210–218.
[14] H. Ait-Amokhtar, P. Vacher, S. Boudrahem, Kinematics fields and spatial activity of Portevin-Le Chatelier bands using the digital image correlation method, Acta Mater. 54 (2006) 4365–4371.
[15] H. Jiang, Q. Zhang, X. Wu, J. Fan, Spatiotemporal aspects of the Portevin-Le Chatelier effect in annealed and solution-treated aluminum alloys, Scripta Mater. 54 (2006) 2041–2045.
[16] M.S. Bharathi, M. Lebyodkin, G. Ananthakrishna, C. Fressengeas, L.P. Kubin, The hidden order behind jerky flow, Acta Mater. 50 (2002) 2813–2824.
[17] L.P. Kubin, C. Fressengeas, G. Ananthakrishna, F.R.N. Nabarro, M.S. Duesbery (Ed.), Dislocations in Solids, vol 11, Elsevier Science B.V., Amsterdam, 2002, p. 101.
[18] S. Kok, M.S. Bharathi, A.J. Beaudoin, C. Fressengeas, G. Ananthakrishna, L.P. Kubin, M. Lebyodkin, Spatial coupling in jerky flow using polycrystal plasticity, Acta Mater. 51 (2003) 3651–3662.
[19] Q. Hu, Q. Zhang, P. Cao, S. Fu, Thermal analyses and simulations of the type A and type B Portevin-Le Chatelier effects in an Al-Mg alloy, Acta Mater. 60 (2012) 1647–1657.
[20] A. Chrysochoos, H. Louche, An infrared image processing to analyse the calorific effects accompanying strain localisation, Inter. J. Eng. Sci. 38 (2000) 1759–1788.
[21] M. Lebyodkin, Y. Bréchet, Y. Estrin, L.P. Kubin, Statistical behaviour and strain localization patterns in the Portevin-Le Chatelier effect, Acta Mater. 44 (1996) 4531–4541.
[22] M. Lebyodkin, L. Dunin-barkowskii, Y. Bréchet, Y. Estrin, L.P. Kubin, Spatio-temporal dynamics of the Portevin-Le Chatelier effect: experiment and modelling, Acta Mater. 48 (2000) 2529–2541.